The Journal of Chemical Physics

RESEARCH ARTICLE | JULY 16 2025

Quantification of the basis set error for molecules in strong magnetic fields and general orientation

Raunak Farhaz ; Florian A. Bischoff ; Simon Blaschke ; Stella Stopkowicz

J. Chem. Phys. 163, 034308 (2025)
https://doi.org/10.1063/5.0274736

The Journal of Chemical Physics ARTICLE pubs.aip.org/aip/jcp

Quantification of the basis set error for molecules in strong magnetic fields and general orientation

Cite as: J. Chem. Phys. 163, 034308 (2025); doi: 10.1063/5.0274736
Submitted: 8 April 2025 • Accepted: 16 June 2025 •
Published Online: 16 July 2025

Raunak Farhaz,[1,a] Florian A. Bischoff,[1,b] Simon Blaschke,[2,3,c] and Stella Stopkowicz[3,4,d]

AFFILIATIONS

[1] Institut für Chemie, Humboldt-Universität zu Berlin, Unter den Linden 6, 10099 Berlin, Germany
[2] Department Chemie, Johannes Gutenberg-Universität Mainz, Duesbergweg 10-14, D-55128 Mainz, Germany
[3] Fachrichtung Chemie, Universität des Saarlandes, Campus B2.2, D-66123 Saarbrücken, Germany
[4] Hylleraas Centre for Quantum Molecular Sciences, Department of Chemistry, University of Oslo, P.O. Box 1033, N-0315 Oslo, Norway

[a] **Electronic mail:** raunak.farhaz@hu-berlin.de
[b] **Author to whom correspondence should be addressed:** florian.bischoff@hu-berlin.de
[c] **Electronic mail:** siblasch@uni-mainz.de
[d] **Electronic mail:** stella.stopkowicz@uni-saarland.de

ABSTRACT

The paper investigates the basis set incompleteness errors of the Hartree–Fock energies for molecules in extreme magnetic field strengths up to $5B_0$ ($\approx 10^6$ T), considering electronic state, geometric structure, and orientation of the molecule with respect to the magnetic field. We compare the results from finite-field calculations using uncontracted correlation-consistent basis sets with the fully numerical solution using multiresolution analysis on the He atom and its dimer, as well as the methylidyne radical and the water molecule. Standard uncontracted aug-cc-pVQZ basis sets are generally reliable up to $B = 0.2B_0$. Between $B = 0.5B_0$ and $1.0B_0$, care must be taken as the ground state switches to states with high multiplicities, for which standard basis sets have not been optimized. Beyond $B = 1.0B_0$, the angular and state dependence of these basis sets becomes too large and too unsystematic for results to be considered reliable.

I. INTRODUCTION

Atoms and molecules exposed to strong magnetic fields on the order of one atomic unit, $B_0 \approx 235$ kT, dramatically change their chemistry and physics. For example, new bonding mechanisms, like perpendicular paramagnetic bonding, can occur for molecules with a formal bond order of zero.[1,2] Furthermore, the ordering of electronic states might change, electron densities are strongly deformed, and high-spin states can be energetically favored over low-spin states. Such strong fields occur on white dwarf stars, which often have hydrogen or helium atmospheres,[3,4] but, as has been shown recently, can also contain heavier elements.[5] Even stronger magnetic fields (much) larger than $1B_0$ occur on neutron stars and magnetars.[3] For atoms as well as for linear molecules oriented parallel to the magnetic field, highly accurate numerical computations can be performed by taking advantage of the cylindrical symmetry of the system.[6–15] For the special case of extremely strong fields, like those on neutron stars, calculations have been performed based on an expansion of Landau states.[16] In addition, specialized numerical atomic codes have also been presented.[17,75]

In 2008, Tellgren *et al.*[18] presented an implementation based on London orbitals[19] that laid the foundation for the study of molecules in a general orientation of the magnetic field. Standard quantum chemical basis sets are not well suited for strong magnetic fields, as they cannot properly adapt to the shape of the external potentials.[20,21] Today, in respective calculations in the regime of up to $1B_0$, large uncontracted Gaussian basis sets are employed.

The problem of the incomplete basis set becomes even more severe when the molecule is not oriented along the magnetic field vector. In this case, even for fixed field strengths, electronic states, and interatomic distances, the total energy as well as the basis set error might change as a function of the direction of the magnetic

field. Anisotropic Gaussian basis sets have been proposed to alleviate the problem[22,23] for arbitrary orientations of the molecules with respect to the magnetic field vector. The results are quite promising; however, this approach requires field-dependent optimizations as well as the use of new integral codes, which are still non-standard and may well still lead to very large or very system-dependent basis sets.

Basis-set studies have been performed for atoms[12,13,21,24] and molecules.[15,18,25] Overall, they have indicated that for up to $1B_0$, the use of large uncontracted basis sets is adequate.[18,25] In numerical calculations for linear molecules in parallel fields, it was shown that for fields of around $10B_0$, basis set errors of up to 1000 kcal/mol can occur.[15] In addition, the basis set incompleteness error (BSIE) is not systematic, and oscillations may occur when the magnetic field is increased.[15]

Lehtola *et al.*[15] report a rapidly growing BSIE with the magnetic field strength, ranging from 1 mE_h in the field-free case to errors larger than $1.0E_h$ for the strongest fields considered, that is, $10B_0$. In addition to the increase of the BSIE with field strength, they report an increase of the BSIE with increasing multiplicity by an order of magnitude. This increase is due to the fact that higher-angular momentum functions are absent in the LCAO approach to describe the relevant states for such multiplicities and field strengths. This was recently further affirmed by Ref. 24. Thus, they conclude that using the LCAO approach with standard basis sets, reliable results can only be obtained up to magnetic field strengths of $1.0B_0$. These calculations were limited, however, to the parallel orientation of the magnetic field, that is, to cylindrical symmetry.

In this paper, we assess the BSIE of molecules in an arbitrary orientation of the magnetic field by comparing the results from Hartree–Fock calculations based on large uncontracted basis sets from London orbitals with numerical calculations using multiresolution analysis.[26] In particular, we investigate the helium dimer potential energy surfaces in arbitrary orientations to the magnetic field, as well as the CH radical and the water molecule in various field orientations for field strengths up to $5B_0$.

II. METHODOLOGY

A. The Hamiltonian for a molecule in a magnetic field

A static uniform magnetic field can be introduced into the electronic Hamiltonian by substituting the canonical momentum $\boldsymbol{p}$ with the kinetic momentum $\boldsymbol{\pi} = \mathbf{p} + \mathbf{A}$, where $\mathbf{A}$ is the vector potential:

$$\hat{H} = \frac{1}{2m}(\mathbf{p} + \mathbf{A})^2 + \hat{V}_{ee} + \hat{V}_{ne} + \hat{V}_{nn}. \tag{1}$$

The potential terms $\hat{V}$ describe the electron–electron interaction, the electron–nuclear interaction, and the nuclear–nuclear interaction, respectively. Expanding the square of the kinetic momentum operator, using the Coulomb gauge, $\nabla \cdot \mathbf{A} = 0$, and assuming a homogeneous magnetic field along the z-axis, leads to an expression for the Hamiltonian with additional potential-like terms:

$$\hat{H} = \hat{T} + \frac{1}{2}B\hat{L}_{\boldsymbol{O},z} + B\hat{S}_z + \frac{1}{8}B^2(x_{\boldsymbol{O}}^2 + y_{\boldsymbol{O}}^2) + \hat{V}_{ee} + \hat{V}_{ne} + \hat{V}_{nn}, \tag{2}$$

where the second, third, and fourth terms correspond to the orbital-Zeeman term, spin-Zeeman term, and diamagnetic potential, respectively. The subscript $\boldsymbol{O}$ designates the gauge origin of the magnetic field.

The expectation value of the $\boldsymbol{\pi}^2$ operator is invariant with respect to the movement of the gauge origin. This is, however, not the case for the corresponding individual contributions. As seen from Eq. (2), both the orbital-Zeeman term and the diamagnetic term are gauge-origin dependent. Calculations using finite basis sets are hence gauge-origin dependent as well. This issue can be resolved either by using a complete basis set, as done in multiresolution analysis (MRA),[27] or by using gauge including atomic orbitals (GIAO)[19] in calculations that employ a linear combination of atomic orbitals (LCAO). In contrast to field-free calculations, the wave functions are complex in a finite field.

B. Linear combination of atomic orbitals

Using the linear combination of atomic orbitals (LCAO) approach, the one-electron wave function is represented in a finite basis set. The spatial part of the spin orbitals $\varphi_i(\boldsymbol{r}, \sigma) = \phi_i(\boldsymbol{r})s_i(\sigma)$ can be expanded as a linear combination of N atomic orbitals (AOs) $\chi_\mu(\boldsymbol{r})$, which are weighted by the respective expansion coefficient, $c_{\mu i}$, that is,

$$\phi_i(\boldsymbol{r}) = \sum_{\mu}^{N} c_{\mu i}\chi_\mu(\boldsymbol{r}). \tag{3}$$

In this study, Gaussian basis sets are employed.[28] For this choice, the AO basis functions are described by Gaussian-type orbitals (GTO). A Cartesian GTO,

$$\chi_\mu(\boldsymbol{r}) = N_\mu x_\mu^{n_\mu} y_\mu^{l_\mu} z_\mu^{m_\mu} \mathrm{e}^{-\alpha_\mu \boldsymbol{r}_\mu^2}, \tag{4}$$

is defined by a normalization constant N_μ, a polynomial of Cartesian coordinates that describes the angular dependency for a given angular momentum (in the Cartesian basis) $L = n_\mu + l_\mu + m_\mu$ and a radial part parameterized by a Gaussian exponential depending on the distance $\boldsymbol{r}_\mu = \boldsymbol{r} - \boldsymbol{R}_\mu$ with the center of the basis function $\boldsymbol{R}_\mu$.

To ensure gauge-origin invariance when treating the system within a magnetic field $\boldsymbol{B}$, the correct transformation behavior with respect to the transformation of the gauge origin $\boldsymbol{O}$ is introduced by dressing the Gaussian basis set with a plane-wave London phase factor.[18,19,29] The resulting London orbitals, which are synonymous with GIAOs, are then defined as

$$\omega_\mu(\boldsymbol{r}) = \mathrm{e}^{-i\boldsymbol{k}_\mu \cdot \boldsymbol{r}}\chi_\mu(\boldsymbol{r}), \tag{5}$$

where the wave vector $\boldsymbol{k}_\mu$ of the phase factor is given by

$$\boldsymbol{k}_\mu = \frac{1}{2}\boldsymbol{B} \times (\boldsymbol{R}_\mu - \boldsymbol{O}). \tag{6}$$

The first implementation making use of London orbitals for the treatment of molecules in strong magnetic fields in the context of Hartree–Fock (HF) theory was been presented in Ref. 18. Since then, a plethora of further quantum-chemical methods in finite magnetic fields, including full configuration interaction,[1] coupled cluster theory,[25,30–34] second-order Møller–Plesset perturbation theory,[33,35] density-functional theory,[36–38] GW[39] and GW/BSE[40] approaches, and others,[41–45] have been developed.

C. Multiresolution analysis

Multiresolution analysis (MRA)[46–48] is the technique of mapping arbitrary multivariate functions and operators into adaptive sets of boxes with polynomials $\phi_{kl}^{n}(x)$ (here in one dimension):

$$f(x) = \sum_{nl}^{k_{\max}-1} \sum_{k=0} \phi_{kl}^{n}(x) s_{kl}^{n}. \tag{7}$$

The parameter $k_{\max}$ is the number of polynomials in each box, $l = 0, \ldots, 2^{n-1}$ is a translation index, and n is the refinement level. If the maximum polynomial order is chosen to be small, the algorithm will subdivide the boxes with large errors more often (larger n), and vice versa, such that the overall precision is always met.

A number of operations can be defined in this basis, including addition, pointwise multiplication, differentiation, and fast application of an integral operator.[49] After rewriting the Schrödinger equation (or its approximations used in quantum chemistry) as an integral equation,

$$(\hat{T} + \hat{V})\Psi = E\Psi \Leftrightarrow \Psi = -\left(\hat{T} - E\right)^{-1} \hat{V}\Psi, \tag{8}$$

MRA can be used to solve for approximate solutions to the Schrödinger equation to finite, but arbitrary precision.

This unique feature allows us to compute arbitrary functions without using a predefined set of basis functions, which usually come with high efficiency but also a number of drawbacks—e.g., inappropriate design for the particular property of interest or near-linear dependencies that can hamper convergence. MRA thus effectively eliminates one of the two major sources of error in electronic structure theory: the basis set incompleteness error (BSIE). By virtue of being at the limit of the complete basis, no errors stemming from the gauge-origin dependence of the Hamiltonian occur at the MRA level. Therefore, a GIAO-like treatment is not necessary—or even possible—as no atomic basis functions are used.

In quantum chemistry, MRA has been used to compute Hartree–Fock wave functions and densities within density functional theory,[46,50] including first and second derivatives[51,52] and excited states,[53,54] and correlated wave functions such as MP2 and ground and excited-state coupled cluster.[55–57] MRA has also been used to compute local exchange potentials,[58] in solving the Dirac equation in relativistic quantum chemistry,[59] and as a base method for quantum computing.[60] Most importantly for this paper, MRA has been used to compute the Hartree–Fock wave function for molecules in extreme magnetic fields,[27] where the advantages of the method—namely, the computation at the complete basis limit—were highlighted, manifesting themselves for instance in the absence of gauge-origin dependence and, from a practical standpoint, obtaining the correct orbitals without further considerations of the choice of a suitable basis set.

From Eq. (8), it is evident that the choice of $\hat{V}$ plays a crucial role in formulating the solution to any given problem. For instance, if $\hat{V}$ represents the potential energy function of a simple harmonic oscillator (SHO), it leads to the solution of the SHO eigenvalue problem. In this work, $\hat{V}$ is defined by incorporating the kinetic momentum into the kinetic energy operator $\hat{T}$.[27] The Schrödinger equation using the Hamiltonian of Eq. (2) can be solved in a straightforward manner by adding the orbital-Zeeman term, spin-Zeeman term, and the diamagnetic potential into $\hat{V}$.

III. COMPUTATIONAL DETAILS

HF-LCAO calculations were performed using the program packages LONDON[18,61] and CFOUR.[62,63] To ensure equivalence between both program suites, uncontracted (unc) augmented (aug) Dunning basis sets[64–66] using Cartesian Gaussians were employed throughout this work.

MRA calculations were performed using the ZNEMO[27] module of the MADNESS[26] package, which is publicly available on GitHub.[67] Calculations were performed with a Slater nuclear correlation factor[68] with exponent $a = 2.0$, and with the numerical parameters `econv = 1 × 10^-6`, `k = 9`, and `eprec = 1 × 10^-6`. To enhance convergence, the potential and the wave functions were damped to zero at a cutoff radius, chosen large enough to not affect the physics of the system. For details, see Ref. 27.

IV. RESULTS AND DISCUSSION

A. Total energies for the helium atom

The total energies of the He atom are computed at the Hartree–Fock (HF) level of theory for various spin multiplicities and magnetic field strengths B using MRA as well as LCAO in an uncontracted quadruple-zeta basis set with both single and double augmentation, denoted as unc-aug-cc-pVQZ and unc-d-aug-cc-pVQZ, respectively. In the triplet cases, the electrons are oriented antiparallel to the magnetic field, thus lowering the total energy via the spin-Zeeman term. Table I shows the total energies of the He atom for the computed states. The term symbols are given for two

TABLE I. Total energies for singlet and triplet states of the He atom in E_h computed with MRA and BSIE in mE_h with respect to the LCAO calculations using unc-aug-cc-pVQZ (*aug*) as well as unc-d-aug-cc-pVQZ (*d-aug*) basis sets.

B/B_0	MRA/E_h				BSIE(*aug*)/mE_h				BSIE(*d-aug*)/mE_h			
State	$^1S_0$	$^3S_0$	$^3P_0$	$^3P_1$	$^1S_0$	$^3S_0$	$^3P_0$	$^3P_1$	$^1S_0$	$^3S_0$	$^3P_0$	$^3P_1$
$C_{\infty h}$	$^1\Sigma_g$	$^3\Sigma_g$	$^3\Sigma_u$	$^3\Pi_g$	$^1\Sigma_g$	$^3\Sigma_g$	$^3\Sigma_u$	$^3\Pi_g$	$^1\Sigma_g$	$^3\Sigma_g$	$^3\Sigma_u$	$^3\Pi_g$
0.0	−2.861 680	−2.174 251	−2.131 456	−2.131 442	0.1	2.8	77.7	77.7	0.1	0.2	2.5	2.5
0.5	−2.814 450	−2.452 834	−2.477 331	−2.615 550	0.2	48.8	33.4	8.7	0.1	9.6	11.7	2.4
1.0	−2.688 885	−2.649 181	−2.730 170	−2.959 685	0.3	156.8	66.3	33.9	0.2	84.5	14.1	4.3
2.0	−2.289 143	−2.998 237	−3.130 764	−3.502 050	1.5	288.8	138.4	28.2	1.4	282.9	74.7	20.5
5.0	−0.532 435	−3.766 603	−3.953 974	−4.617 249	15.0	1306.2	231.7	81.4	14.7	1285.6	231.7	79.5

different symmetries, that is, spherical/field-free and the physical point group $C_{\infty h}$.

It was shown in Ref. 25 that double augmentation is required in order to describe the p functions in the $^3P_0(^3\Sigma_u)$ correctly already in the field-free case. This is, however, a special case for helium. For most other systems, it was shown that uncontracted singly augmented basis sets are sufficient for field strengths up until $1.0B_0$.[25] Accordingly, the errors for the $^3P_0(^3\Sigma_u)$ and $^3P_1(^3\Pi_g)$ states are significantly decreased when going from single to double augmentation, while they are nearly unchanged for the $^1S_0(^1\Sigma_g)$ state. For the states $^3S_0$ $(^3\Sigma_g)$, $^3P_0$ $(^3\Sigma_u)$, and $^3P_1$ $(^3\Pi_g)$, the total energies using MRA are between 1 and 250 mE_h lower than the LCAO values, with errors rising with increasing magnetic-field strength B. The state $^3S_0$ $(^3\Sigma_g)$, however, is an outlier, as the $2s$ orbital (in field-free notation) changes in character from s to d shape (both s and d_0 are of σ symmetry in the magnetic field and may hence mix; see for example Ref. 31), as shown in Fig. 1. Neither of the two basis sets can describe this state adequately. In fact, the basis set would need to contain at least diffuse d, as well as polarizing g and i functions that are not present in standard basis sets; due to inversion symmetry, the necessary l quanta increase in steps of 2.

Our results are in line with the total energies computed in Ref. 24, where magnetic field strengths of up to $0.6B_0$ were considered and numerical results were compared to GTO calculations. Note that the state $\sigma^{2,0}$ of Table S2 of Ref. 24 can correspond to both $^3\Sigma_g$ and $^3\Sigma_u$ states. It was noticed that in the uncontracted aug-cc-pVTZ basis set, the $^3\Pi_g$ states are described better with increasing magnetic field, but the $^3\Sigma_g$ state becomes worse. A figure of the development of the energy of the states with respect to the B field is given in the supplementary material (refer to Fig. 1).

B. Potential energy surfaces for the He dimer

The potential energy surfaces of the He_2 molecule[69] are plotted in Figs. 2–4. For both MRA and LCAO, total electronic energies are plotted against the respective dissociation limit computed from Table I for the basis sets unc-aug-cc-pVQZ and unc-d-aug-cc-pVQZ. Minimum structures and energies are given in Tables II–IV. In the following, we will use the term symbols for the parallel orientation of the molecule with respect to the magnetic field for clarity, keeping in mind that for all tilted orientations, the symmetry is decreased to C_i. For an in-depth discussion of the development of low-lying excited states of the He_2 molecule at field strengths of 0.2 and $1.0B_0$, we refer the reader to Ref. 69.

1. Singlet

For all magnetic field strengths, the singlet He dimer dissociates into two $^1S_0$ $(^1\Sigma_g)$ atoms. As anticipated, in the field-free case, the LCAO and MRA energies are very similar. Only at very short distances do the LCAO calculations show a negligible error compared to the MRA calculations of <1 mE_h. With increasing magnetic field strength, an angular dependence on both energies and energy differences occurs. At $B = 1.0B_0$, perpendicular paramagnetic bonding is observed with a bond length of $\approx 3.4a_0$,[1] but the geometry quickly changes away from the perpendicular orientation as the magnetic field increases toward $B = 5.0B_0$. While the perpendicular bonding mechanism favors a perpendicular orientation of the

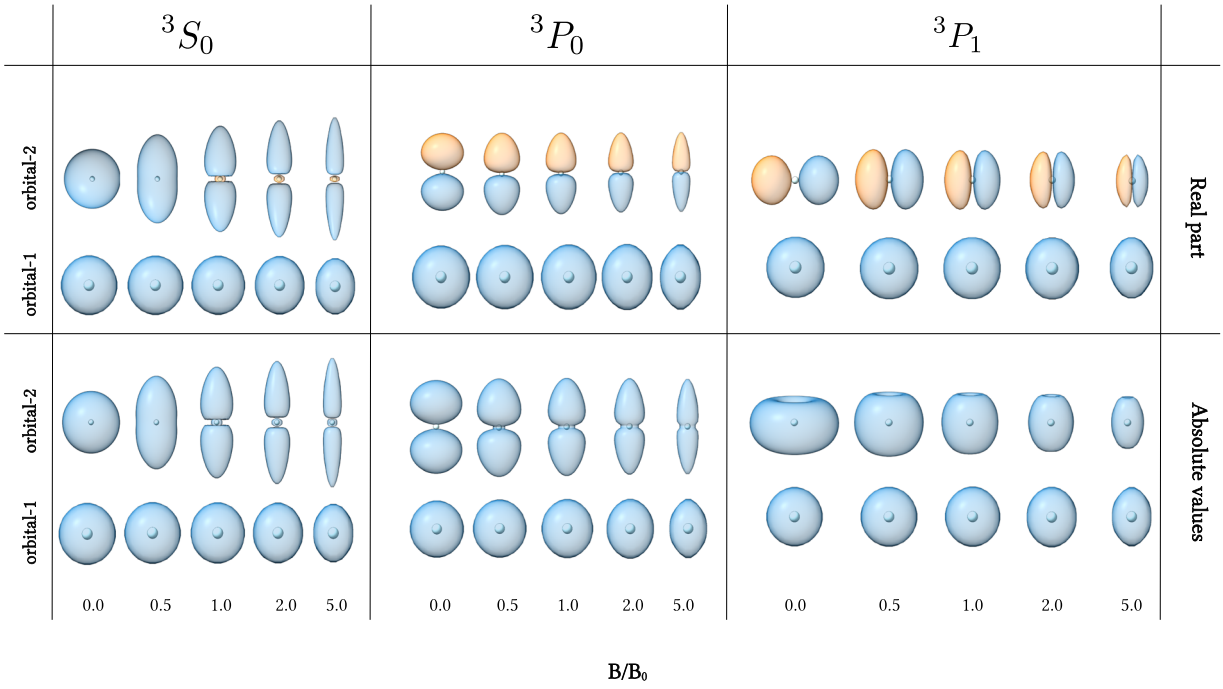

FIG. 1. Hartree–Fock orbitals of the He atom in its singlet and triplet spin states and different magnetic field strengths from MRA calculations.

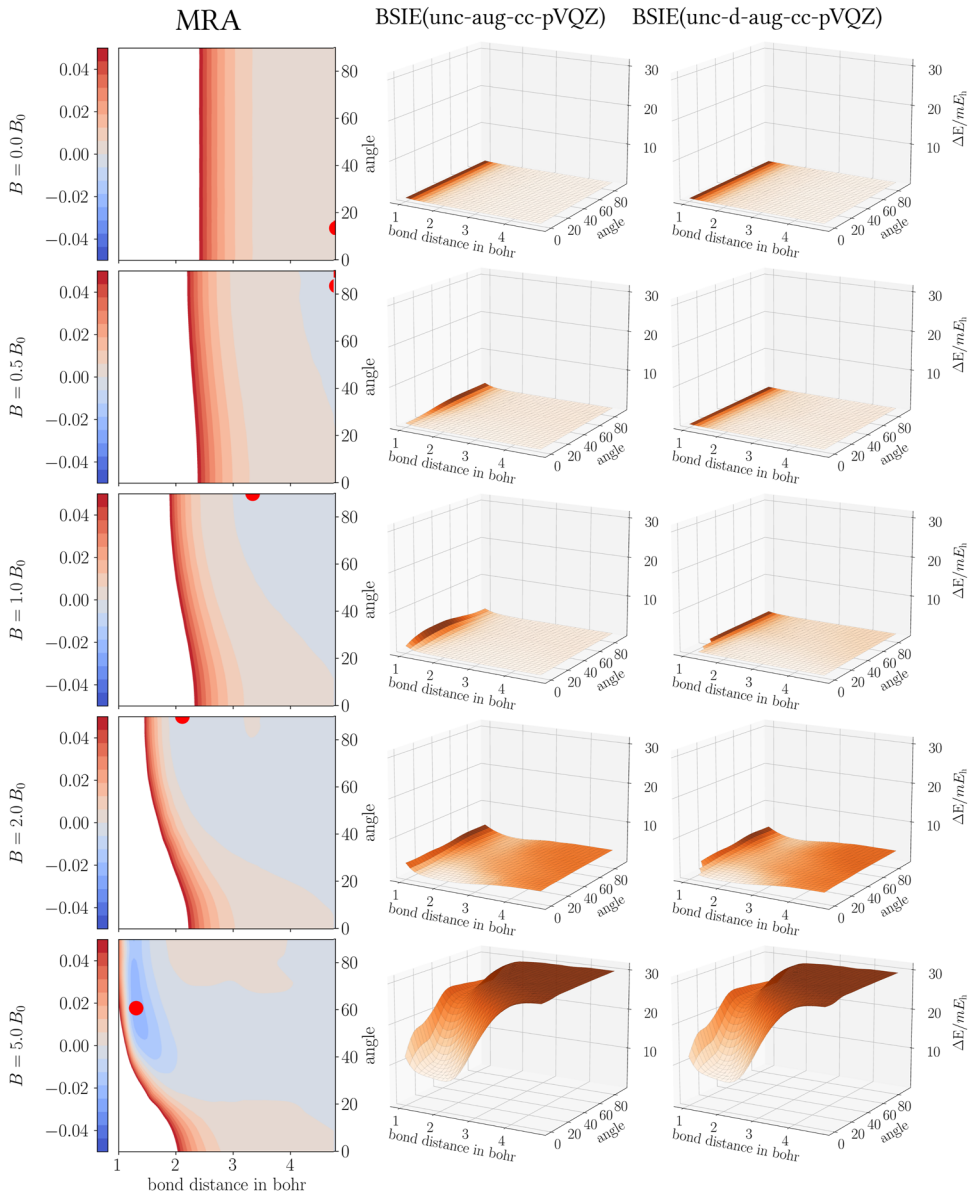

FIG. 2. Singlet He dimer PES; [left to right] **first column**: *relative energies in* E_h; **second column** and **third column**: *BSIE in* mE_h.

molecule, the diamagnetic potential has a minimum at the parallel orientation, eventually forcing the molecule into a parallel orientation with increasing field strength. A similar behavior has already been reported for the lowest triplet state of H_2.[22]

The difference plots in the third column confirm the previous assumption that large basis set calculations are mostly reliable up to $B = 1.0B_0$, but not beyond that.[18,25] At $B = 5.0B_0$, the BSIE increases up to 30 mE_h (at a bond strength of 39 mE_h), and it is strongly dependent on angle and bond distance. Overall both basis sets are adequate up to $B = 2.0B_0$ and are similarly poor for $B = 5.0B_0$. The additional augmentation has little effect on the PES.

2. Triplet

The triplet helium dimer shows a symmetry-breaking behavior at long distances as the system will dissociate into a singlet and a triplet He atom. For the field-free case, it is $^1S_0$ ($^1\Sigma_g$) and $^3S_0$ ($^3\Sigma_g$), and for $B \geq 0.5B_0$, it is $^1S_0$ ($^1\Sigma_g$) and $^3P_1$ ($^3\Pi_g$). In the following, we will discuss the system dissociating into two symmetric fragments rather than the broken-symmetry solution with distinct singlet and triplet fragments, as both solutions differ only in the dissociation limit, while the main features of the PES at short distances are identical. In the field-free case, the lowest-lying triplet state is the $^3\Sigma_u$ state

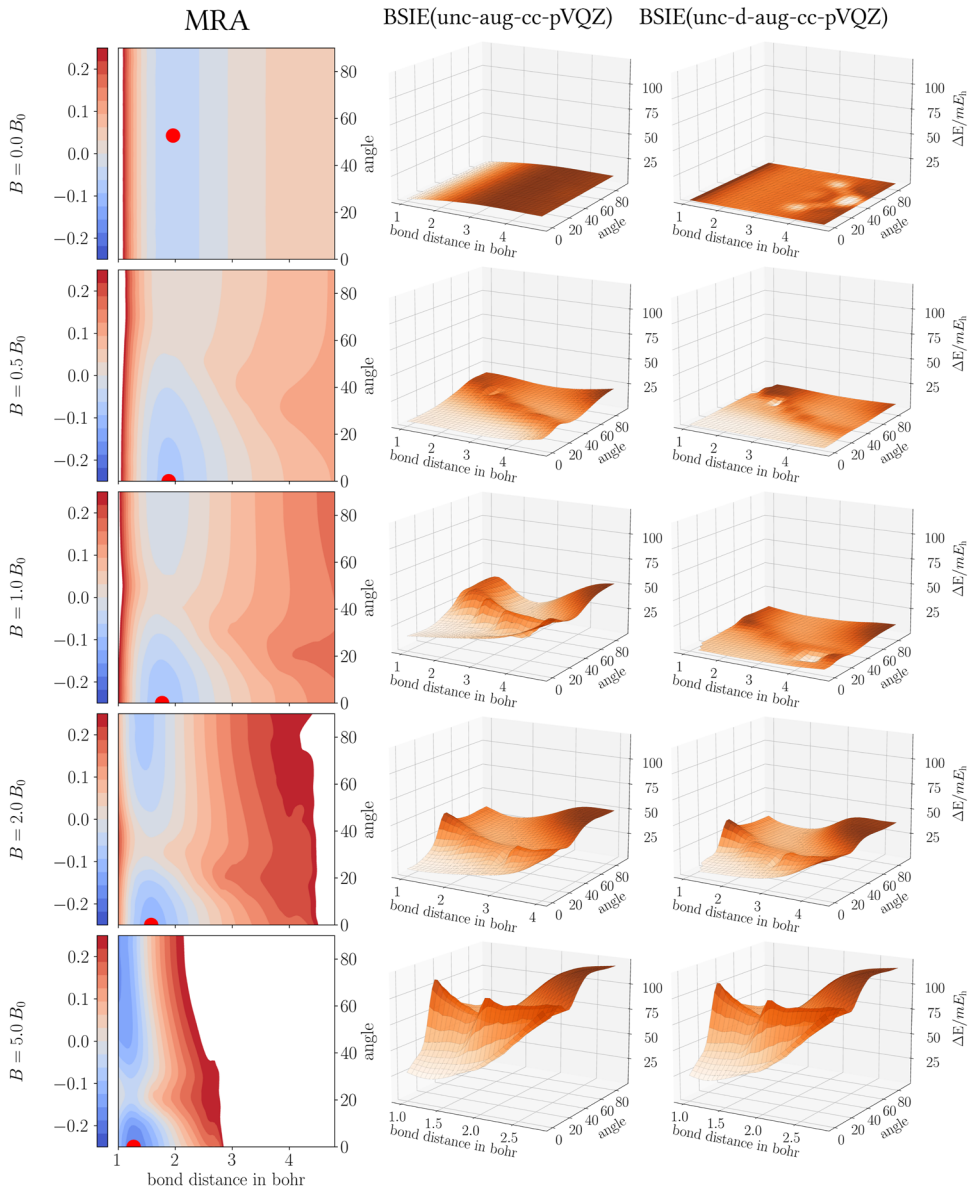

FIG. 3. Triplet He dimer PES; [left to right] **first column**: *relative energies in* E_h; **second column** and **third column**: *BSIE in* mE_h.

with occupation $\sigma_g^2\ \sigma_u^1\sigma_g^1$. There is a bond with a minimum of 49 mE_h at the equilibrium distance of 2.0 a_0.

Already at small magnetic field strengths, the $^3\Pi_g$ state with occupation $\sigma_g^2\sigma_u^1\pi_{u,-1}^1$ is lower in energy for the (near) parallel orientation up to $\theta = 70°$ due to stabilization by the orbital-Zeeman term. At a magnetic field strength of $B = 0.5B_0$, the $^3\Sigma_u$ state is completely repulsive. At $B = 1.0B_0$, a minimum is observed again. Interestingly, with increasing magnetic field strength, the angle at which $^3\Pi_g$ is more stable than $^3\Sigma_u$ decreases to $\theta = 25°$. The two states show different basis set errors; on an average, the $^3\Sigma_u$ state has a larger BSIE than the $^3\Pi_g$ state. This is in line with the atomic calculations, where the $^3\Pi_g$ state is better described than the $^3\Sigma_g$ state in all basis sets and at all magnetic field strengths greater than zero (see Table I).

The additional augmentation functions of the unc-d-aug-cc-pVQZ basis set reduce the BSIE especially at $B = 1.0B_0$, due to the improved description of the π_u^1 orbital, similar to the atomic calculations. For stronger magnetic fields, the additional functions have less effect. At field strengths greater than $1.0B_0$, both basis sets have a strong BSIE along both the angular and the dissociative direction, reaching up to 70 mE_h.

3. Quintet

For $B = 0.0B_0$, the quintet state dissociates into two $^3S_0$ He atoms, while for higher magnetic field strengths, it dissociates into two $^3P_1$ He atoms. For $B = 0.0B_0$, the quintet state shows a small apparent minimum: the ground-state configuration changes from

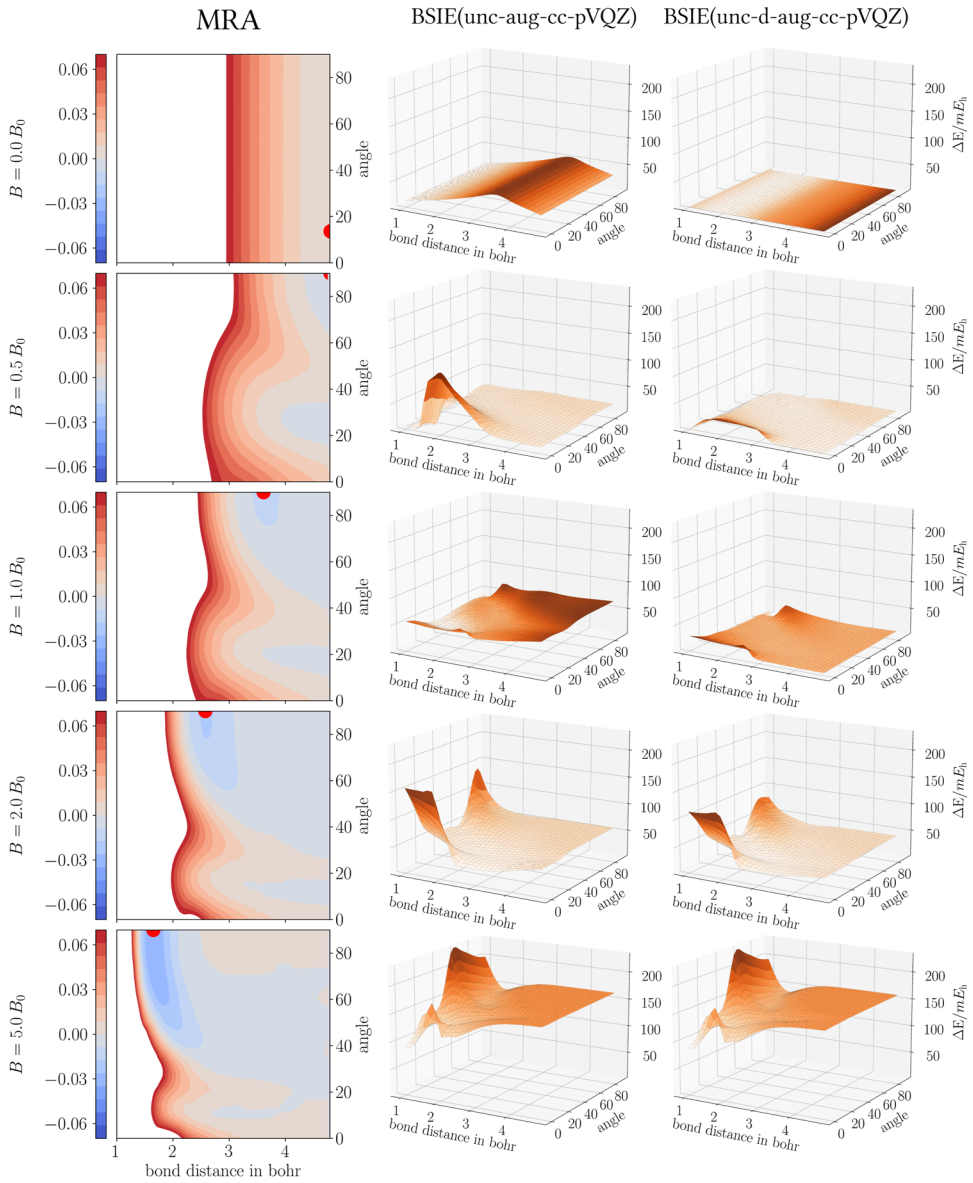

FIG. 4. Quintet He dimer PES; [left to right] **first column**: *relative energies in* E_h; **second column** and **third column**: *BSIE in* mE_h. For the cusp in the energy differences at $B = 0.0B_0$, see text.

$^5\Pi_g(\sigma_g^1\sigma_u^1\sigma_g^1\pi_{-1,u}^1)$ to $^5\Sigma_g^+(\sigma_g^1\sigma_u^1\sigma_g^1\sigma_u^1)$ with increasing distance, with the crossover point at 6.5 a_0 in MRA, but 3.6 a_0 in LCAO in the unc-aug-cc-pVQZ basis. The distinctive cusp in the difference plot of Fig. 4 in the singly augmented basis set can therefore be traced back to the swapping of the ground state and the poor description of the π orbital in this basis set. When the second set of diffuse functions is added (i.e., using the unc-d-aug-cc-pVQZ basis), the π orbital is stabilized and the dissociation curve is close to the MRA one, as seen in Fig. 5.

With increasing magnetic field strengths, the ground state is described by the $^5\Pi_g(\sigma_g^1\sigma_u^1\pi_{-1,u}^1\pi_{-1,g}^1)$ state, changing to the $^5\Phi_g(\sigma_g^1\sigma_u^1\pi_{-1,u}^1\delta_{-2,g}^1)$ state for small bond lengths ($R < 2.0a_0$ at $B = 0B_0$ and decreasing with increasing field strengths). The relevant part of the PES is described by the $^5\Pi_g$ state, showing two competing minima.[69] The BSIE leaves the LCAO calculation predicting the wrong global minimum for $B = 0.5B_0$ and $B = 1.0B_0$ for unc-aug-cc-pVQZ, namely, predicting a tilted geometry with an angle of 20°–30°, while MRA predicts a perpendicular bond (refer to Table IV and Fig. 4 in the supplementary material). Both minima are nearly degenerate.

At the strongest magnetic field of $B = 5.0B_0$, the LCAO calculations predict a local minimum at around $r = 2.42a_0$ and $\theta = 11°$ (for unc-aug-cc-pVQZ) and $r = 2.42a_0$ and $\theta = 10°$ (for unc-d-aug-cc-pVQZ), which is, however, very shallow in the MRA calculations. In contrast, the MRA calculations still have only a single minimum across the whole PES.

TABLE II. Minimum relative energies for the He dimer for the singlet spin state across magnetic field strengths with MRA and LCAO (unc-aug-cc-pVQZ, unc-d-aug-cc-pVQZ). θ is the angle between the molecular axis of the He dimer and B and r is the bond length of He_2.

	MRA			LCAO(*aug*)			LCAO(*d-aug*)		
B/B_0	r/a_0	$\theta/^\circ$	E/mE_h	r/a_0	$\theta/^\circ$	E/mE_h	r/a_0	$\theta/^\circ$	E/mE_h
0.0	N.A.	N.A.	Dissociative	N.A.	N.A.	Dissociative	N.A.	N.A.	Dissociative
0.5	N.A.	N.A.	Dissociative	N.A.	N.A.	Dissociative	N.A.	N.A.	Dissociative
1.0	3.34	90	−0.2	3.34	90	−0.3	3.34	90	−0.3
2.0	2.11	90	−2.7	2.11	90	−3.6	2.11	90	−3.9
5.0	1.31	61	−23.9	1.31	60	−30.7	1.31	60	−31.1

TABLE III. Minimum relative energies for the He dimer for the spin-symmetric triplet state across magnetic field strengths with MRA and LCAO (unc-aug-cc-pVQZ, unc-d-aug-cc-pVQZ). θ is the angle between the molecular axis of the He dimer and B, and r is the bond length of He_2. Bold numbers denote the global minimum.

	MRA			LCAO(*aug*)			LCAO(*d-aug*)		
B/B_0	r/a_0	$\theta/^\circ$	E/mE_h	r/a_0	$\theta\,(^\circ)$	E/mE_h	r/a_0	$\theta\,(^\circ)$	E/mE_h
0.0	**1.96**	**All**	**−49.3**	**1.96**	**All**	**−46.3**	**2.00**	**All**	**−49.3**
0.5	**1.88**	**0**	**−72.1**	**1.88**	**0**	**−76.7**	**1.88**	**0**	**−73.8**
1.0	**1.77**	**0**	**−85.1**	**1.77**	**0**	**−101.6**	**1.77**	**0**	**−88.4**
	1.77	90	−24.2	1.88	90	−28.1	1.81	90	−24.3
2.0	**1.58**	**0**	**−113.6**	**1.58**	**0**	**−135.9**	**1.58**	**0**	**−129.8**
	1.42	90	−75.9	1.46	90	−77.5	1.42	90	−80.0
5.0	**1.27**	**0**	**−188.4**	**1.27**	**0**	**−260.0**	**1.27**	**0**	**−259.7**
	1.00	76	−162.6	1.00	90	−194.5	1.00	90	−193.3

TABLE IV. Minimum relative energies for the He dimer for the quintet spin state across magnetic field strengths with MRA and LCAO (unc-aug-cc-pVQZ, unc-d-aug-cc-pVQZ). θ is the angle between the molecular axis of the He dimer and B, and r is the bond length of He_2. Bold numbers denote the global minimum.

B/B_0	MRA			LCAO(*aug*)			LCAO(*d-aug*)		
	r/a_0	$\theta\,(^\circ)$	E/mE_h	r/a_0	$\theta\,(^\circ)$	E/mE_h	r/a_0	$\theta\,(^\circ)$	E/mE_h
0.0	N.A.	N.A.	Dissociative	N.A.	N.A.	Dissociative	N.A.	N.A.	Dissociative
0.5	4.45	25	−3.8	**4.46**	**25**	**−6.8**	**4.46**	**25**	**−5.7**
	4.80	**90**	**−4.9**	4.80	90	−3.9	4.80	90	−4.8
1.0	4.07	19	−1.9	**3.61**	**21**	**−16.3**	3.99	19	−3.5
	3.61	**90**	**−10.2**	3.61	90	−16.1	**3.61**	**90**	**−11.9**
2.0	4.07	13	−1.2	3.26	15	−18.1	3.26	16	−12.2
	2.57	**90**	**−18.7**	**2.57**	**90**	**−20.4**	**2.54**	**90**	**−22.5**
5.0	3.03	11	−0.9	2.42	11	−23.3	2.42	10	−24.1
	1.65	**90**	**−34.8**	**1.61**	**90**	**−55.6**	**1.61**	**90**	**−56.4**

As before, especially for large magnetic fields starting from $B = 2.0B_0$, huge BSIEs occur that can go up to 200 mE_h, depending on the state, bond length, and orientation of the molecule. For chemically relevant bond lengths $>1.5a_0$, the non-parallelity error—broadly defined as the difference of the largest and the smallest deviation in the shown PES—is smaller but still leads to incorrectly predicted global minima. The trend of the error rising with the multiplicity continues for the quintet state, as we

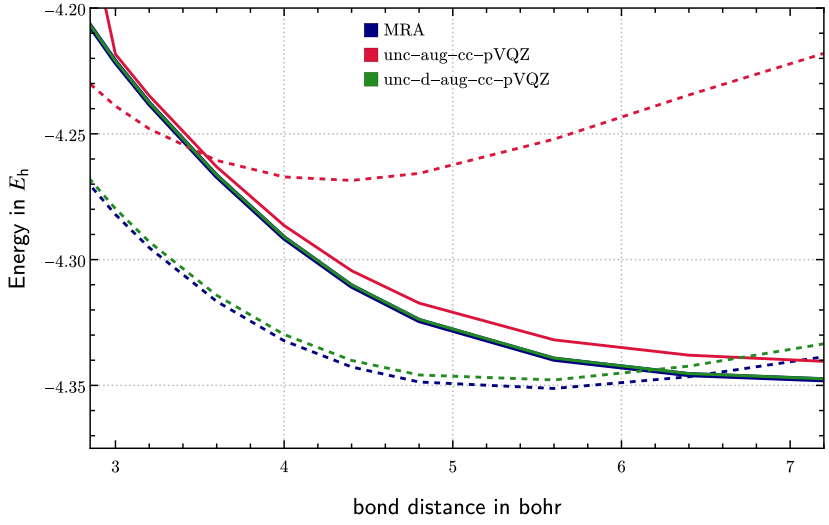

FIG. 5. MRA and LCAO (unc-aug-cc-pVQZ and unc-d-aug-cc-pVQZ) field-free calculations for He_2 in the quintet spin states—$^5\Sigma_g^+(\sigma_g^1\sigma_u^1\sigma_g^1\sigma_u^1)$ (solid) and $^5\Pi_g(\sigma_g^1\sigma_u^1\sigma_g^1\pi_{-1,u}^1)$ (dashed).

observe that the BSIE gets larger by an order of magnitude up to 235 mE_h.

C. Potential energy surface slices of methylidyne radical and water

We continue our study on molecules, namely, the methylidyne radical (CH) and water (H_2O).[34,70] As the number of degrees of freedom increases with the number of atoms, we analyze slices through the full data set (geometry, orientation, electronic state, field strength, and basis set) for computational feasibility. Initially, we consider the field-free HF equilibrium geometries for the respective basis set and observe the PES and the change of the basis set incompleteness errors with respect to the electronic state as well as the magnetic field strength B. In contrast to the He dimer, PES singly augmented basis sets are used, as it was shown that the second set of diffuse functions does not have a significant contribution and the PES is already well described with single augmentation.[18,25]

Subsequently, we keep $B = 1.0B_0$ and the electronic state fixed to the ground state (sextet for CH and quintet for H_2O), while varying the molecular geometry along the normal coordinates Q, which again were determined in the field-free case using the unc-aug-cc-pVTZ basis set. For CH, this involves studying orientations parallel and perpendicular to B and adjusting the bond length. For H_2O, we similarly consider both orientations (B is parallel to the C_2 axis as well as perpendicular to the molecular plane) and modify the structure along the normal coordinates.

1. CH

a. Varying states and magnetic field strengths. Table VI and Fig. 6 show the total energies and the BSIE for a number of basis sets across different spin multiplicities (doublet, quartet, and sextet) and magnetic field strengths up to $B = 2B_0$, accounting for both parallel and perpendicular orientations. Note that in the MRA calculations, it was in one instance, that is, the doublet CH radical in a parallel field of $0.2B_0$, not possible to converge into the $^2\Pi_{-1}$ ground state and instead the higher-lying $^2\Delta_{-2}$ state was obtained. The respective states are energetically very close, as they cross at this field strength and orientation as can be seen in Ref. 34. Since in the LCAO calculations it is more straightforward, due to the use of symmetry and the maximum overlap method (MOM),[71–73] to converge to different desired states, we chose to make the comparisons with respect to the $^2\Delta_{-2}$ state that was obtained in the MRA calculations. We note, however, that the basis set requirements for this state may be more demanding. Table V lists the corresponding ground state for the respective field strength.

As expected, the BSIE increases with increasing magnetic field strength and decreases with increasing basis set size. The BSIE is small and constant within and between different spin states and orientations (<4 mE_h) up to $B = 0.2B_0$. Starting from $B = 0.5B_0$, the sextet state starts to deviate significantly for the parallel orientation between the two approaches, as the ground state is now described by a state with an occupied but poorly described δ orbital. Beyond $B = 1.0B_0$, the errors become very large and arbitrary in some cases across different states and geometries. Comparing the difference between parallel and perpendicular orientation, no systematic trends can be observed in the BSIE.

b. Slice along the bond distance. Scanning the normal mode Q, in this case corresponding to the bond length, from −0.6 Q or $1.357a_0$ to +0.6 Q or $2.509a_0$ for the sextet state at $B = 1.0B_0$ in Table VIII shows the error systematically increasing from short to long bond distances. The non-parallelity error, defined as the difference between the largest and the smallest deviation, is 10 mE_h for the unc-aug-cc-pVTZ basis set. Total energies from MRA calculations and BSIE with respect to the LCAO calculations are given in Table IX and illustrated in Fig. 8.

2. H_2O

a. Varying states and magnetic fields. Table VII and Fig. 7 show the total energies of H_2O for varying magnetic field strengths B up to $5B_0$ and spin multiplicities (singlet, triplet, and quintet), as well as the corresponding BSIE for basis sets ranging from unc-aug-cc-pVDZ to unc-aug-cc-pV5Z. We considered two orientations of the

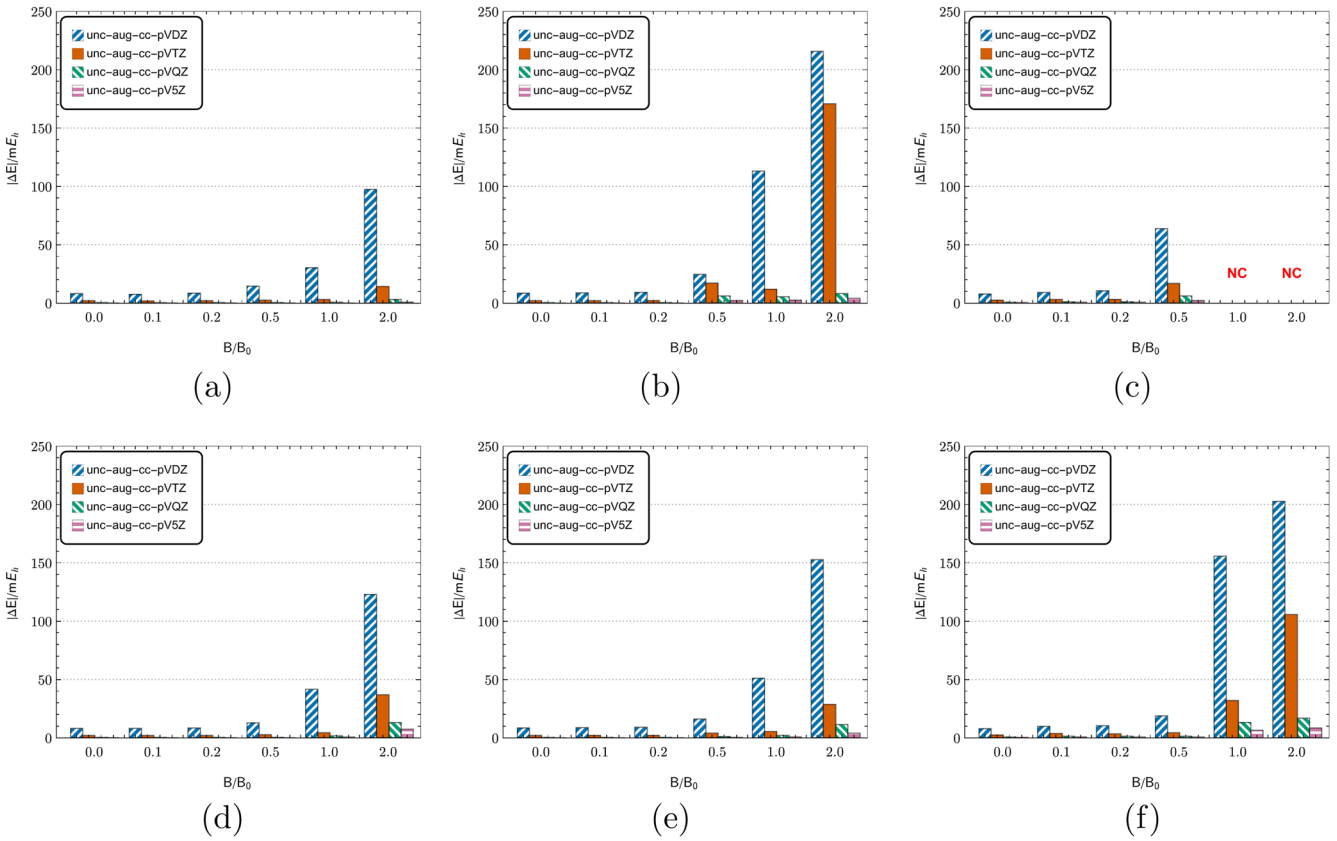

FIG. 6. BSIE of LCAO calculations across unc-aug-cc-pV(D-5)Z basis sets for the CH radical in parallel [(a)–(c)] as well as perpendicular [(d)–(f)] orientation at equilibrium geometry in varying B and S. (a) Doublet CH parallel, (b) quartet CH parallel, (c) sextet CH parallel, (d) doublet CH perpendicular, (e) quartet CH perpendicular, and (f) sextet CH perpendicular.

magnetic field. The first aligns the magnetic field vector along the C_2 axis. In the second orientation, the magnetic field vector is oriented perpendicular to the molecular plane of water.

The overall picture of the BSIE is very similar to the linear CH molecule. For larger basis sets (QZ and 5Z), the BSIE remains below 5 mE_h up until 1.0B_0. In contrast, when employing smaller basis sets (DZ and TZ), the error is considerably larger, reaching values of ~25 mE_h. Beyond B = 1.0B_0, the errors increase dramatically and exhibit substantial fluctuations across different states and geometries, with maximum errors approaching ~1400 mE_h, at which point the calculations become unreliable.

In contrast to the calculations for CH, the MRA calculations for H_2O generally converged well for the magnetic field strengths and orientations considered. However, it is noteworthy that for the

TABLE V. State labels and occupation for the ground state of the CH molecule for varying magnetic field strengths and multiplicities.

B/B_0	Doublet	Quartet	Sextet
0.0	$^2\Pi_{-1}(\sigma^2\sigma^2\sigma^2\pi^1_{-1})$	$^4\Sigma(\sigma^2\sigma^2\sigma^1\pi^1_{-1}\pi^1_{+1})$	$^6\Sigma(\sigma^2\sigma^1\sigma^1\pi^1_{-1}\pi^1_{+1}\sigma^1)$
0.1	$^2\Pi_{-1}(\sigma^2\sigma^2\sigma^2\pi^1_{-1})$	$^4\Sigma(\sigma^2\sigma^2\sigma^1\pi^1_{-1}\pi^1_{+1})$	$^6\Sigma(\sigma^2\sigma^1\sigma^1\pi^1_{-1}\pi^1_{+1}\sigma^1)$
0.2	$^2\Pi_{-1}(\sigma^2\sigma^2\sigma^2\pi^1_{-1})$	$^4\Sigma(\sigma^2\sigma^2\sigma^1\pi^1_{-1}\pi^1_{+1})$	$^6\Sigma(\sigma^2\sigma^1\sigma^1\pi^1_{-1}\pi^1_{+1}\sigma^1)$
0.5	$^2\Delta_{-2}(\sigma^2\sigma^2\sigma^1\pi^2_{-1})$	$^4\Phi_{-3}(\sigma^2\sigma^2\sigma^1\pi^1_{-1}\delta^1_{-2})$	$^6\Delta(\sigma^2\sigma^1\sigma^1\pi^1_{-1}\pi^1_{+1}\delta^1_{-2})$
1.0	$^2\Delta_{-2}(\sigma^2\sigma^2\sigma^1\pi^2_{-1})$	$^4\Phi_{-3}(\sigma^2\sigma^2\sigma^1\pi^1_{-1}\delta^1_{-2})$	$^6\Gamma_{-4}(\sigma^2\sigma^1\sigma^1\pi^1_{-1}\delta^1_{-2}\pi^1_{-1})$
2.0	$^2\Delta_{-2}(\sigma^2\sigma^2\sigma^1\pi^2_{-1})$	$^4\Gamma_{-4}(\sigma^2\sigma^1\sigma^1\pi^2_{-1}\delta_{-2})$	$^6\Gamma_{-4}(\sigma^2\sigma^1\sigma^1\pi^1_{-1}\delta^1_{-2}\pi^1_{-1})$

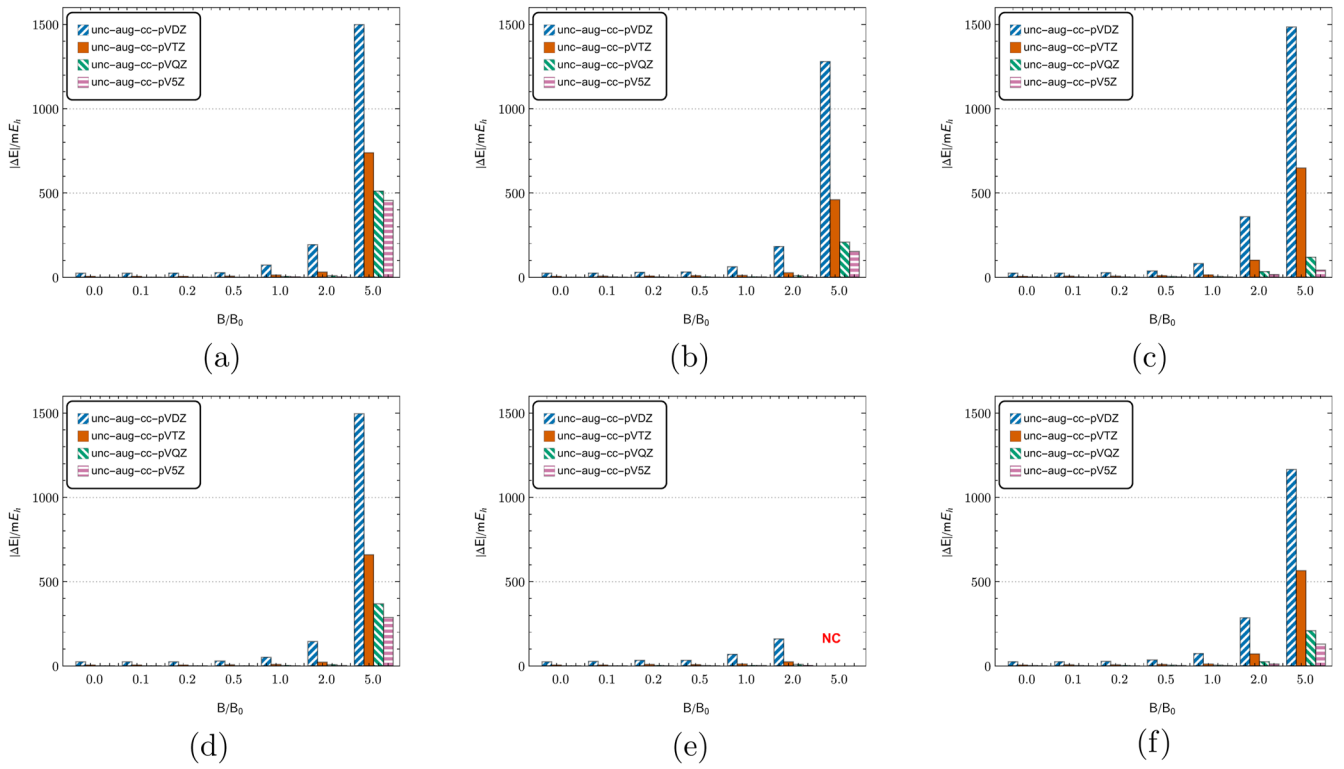

FIG. 7. BSIE of LCAO calculations across unc-aug-cc-pV(D-5)Z basis sets for the H_2O molecule in parallel [(a)–(c)] as well as perpendicular [(d)–(f)] orientation at equilibrium geometry in varying B and S. (a) Singlet H_2O parallel, (b) triplet H_2O parallel, (c) quintet H_2O parallel, (d) singlet H_2O perpendicular, (e) triplet H_2O perpendicular, and (f) quintet H_2O perpendicular.

triplet water calculations, multiple state crossings were observed. Especially in the triplet state and in the orientation where the magnetic field is aligned perpendicular to the molecular plane, we see in LCAO a state crossing where the ground state T_0 at $B = 0.0B_0$ becomes the first excited state at $B = 0.1B_0$ and $B = 0.2B_0$, and then becomes the ground state again at $B = 0.5B_0$. The MRA calculations always converged to the T_0 state in all magnetic field strengths, thus not necessarily to the lowest state. In the LCAO calculations, states can be targeted more directly than in MRA due to the use of symmetry. To compare to the MRA results, we hence converged the calculations to the states that were found with MRA, even if they are not the ground state for the respective field strength and orientation. The absolute energies for both of the triplet states obtained from LCAO calculations are provided in the supplementary material.

b. Slice along the normal modes of vibration. The potential energy surface (PES) slices are examined along the normal modes of vibration, namely symmetric bending, symmetric stretching, and antisymmetric stretching. In all cases, the geometry is distorted about the equilibrium configuration (defined as 0.0 Q). The BSIE is calculated with respect to the unc-aug-cc-pVTZ basis set and is both illustrated in Fig. 8 and tabulated in Table VIII.

For symmetric stretching, as indicated in Table VIII, an increase in the Q value corresponds to an elongation of both O–H bonds. Specifically, the bond length increases from $1.35a_0$ to $2.21a_0$ in steps of $0.14\ a_0$. The mode is dissociative.[73] In addition, the BSIE is observed to decrease, which is consistent with the expectation that the overlap between the atom-centered basis functions diminishes with increasing O–H bond lengths.

In the case of antisymmetric stretching, the behavior of the BSIE is as anticipated. A symmetric pattern is observed, with BSIE taking an identical value of 14.7 mE_h at both extremes (−0.6 Q and +0.6 Q). This outcome is expected, as the geometric structures at these extremes are mirror images of each other. At equilibrium, the error reaches a minimum value of 11.9 mE_h, attributable to the inherent symmetry of the H_2O molecule.

In the case of symmetric bending, both BSIE and the non-parallelity errors are small. However, the form of the curve might be somewhat unexpected, as there is a maximum at the equilibrium geometry. The reference geometry, which is optimized for the field-free singlet water molecule, has bonds too short for the quintet molecule and is therefore at or near a maximum for this mode. The molecule in its quintet state is more stable than in its singlet state, but the quintet state will still dissociate into either a triplet oxygen and two doublet hydrogen atoms, or a triplet oxygen (negative Q) and a triplet hydrogen molecule (positive Q), as seen from the symmetric stretch behavior. Both final dissociation products differ only by 0.2 mE_h.

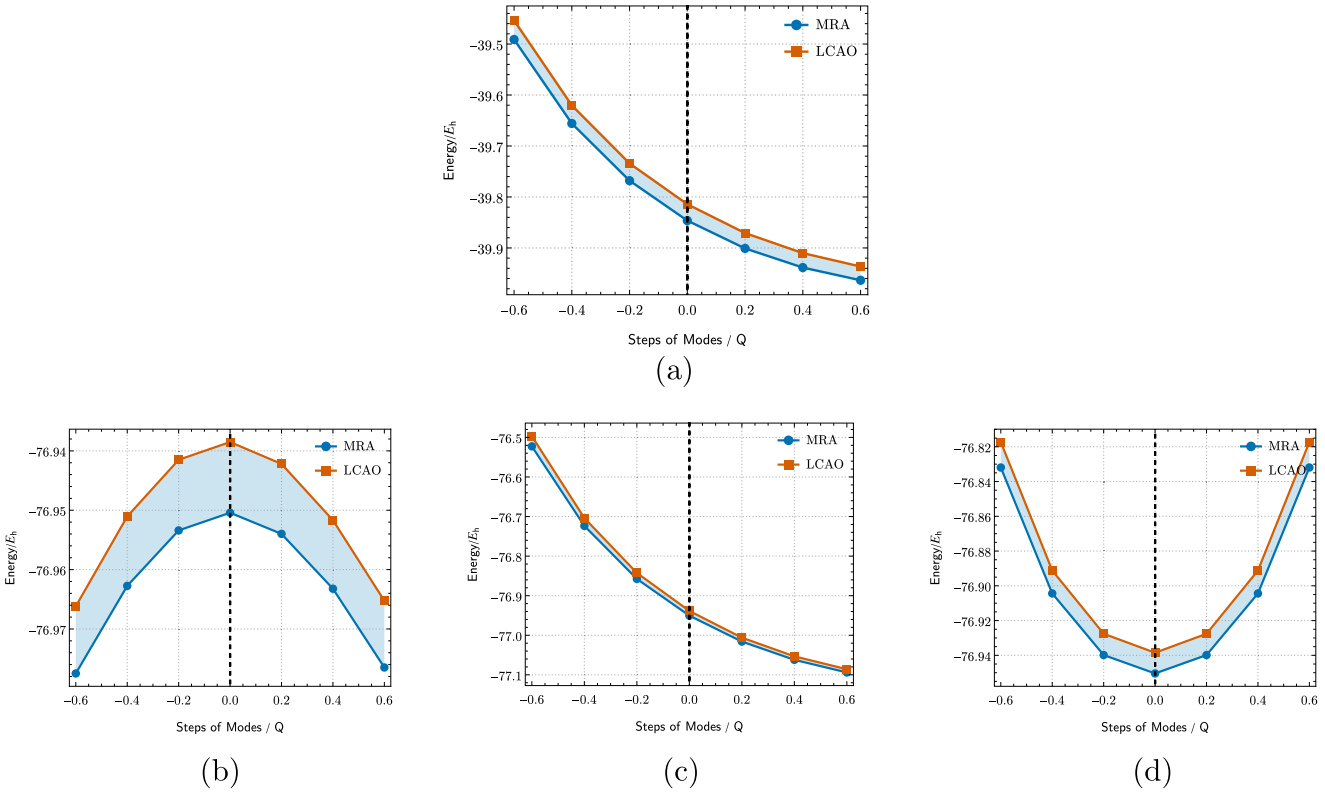

FIG. 8. Total energies for LCAO calculations using unc-aug-cc-pVTZ basis sets as well as MRA for the CH radical in sextet spin state [(a)] and H_2O molecule in its quintet spin state [(b)–(d)] along normal modes of vibration with perpendicular orientation at $B = 1.0B_0$. (a) Symmetric stretching of CH, (b) symmetric bending of H_2O, (c) symmetric stretching of H_2O, and (d) anti-symmetric stretching of H_2O.

V. CONCLUSIONS AND OUTLOOK

In this article, we have studied the basis set incompleteness error (BSIE) for atoms and molecules in extreme magnetic fields at the Hartree–Fock level. The higher the magnetic field strength, the more strongly the electronic states are affected. The electron density becomes more compact in the orientations perpendicular to the magnetic field and typically stretched along the field direction.

In the external magnetic field, states of high angular momentum and multiplicity are stabilized, but they are not well described using standard basis sets. In the field-free case, these problems are encountered rarely and are less severe, as they mainly affect highly excited states. Furthermore, to describe the anisotropy induced by the magnetic field, large uncontracted basis sets are required. In addition, an angular dependence of the molecule with respect to the field emerges, which can affect the BSIE significantly.

As a rule of thumb, we find that standard basis sets, even if uncontracted, can describe the electronic state reliably (i.e., with an error comparable to the field-free calculation) up to $0.2B_0$. From $0.5B_0$, the error sharply increases (by 50% and more), but the physics is still described correctly up to $\sim 1.0B_0$. Beyond that, the errors become too large and too arbitrary for an LCAO treatment. Of course, no sharp line can be drawn here, and what constitutes an acceptable error depends on the system under consideration.

Typically, the correlation energy is on the order of 1% of the total energy. For the systems considered here, for example, water, this corresponds to more than 250 mE_h, making the neglect of electron correlation as severe as the error source of the BSIE. However, once electron correlation is considered, the basis set requirements are even more severe, similar to the field-free case, and even larger uncontracted basis sets are required. To assess the correlated BSIE, an implementation of MP2 or CC in MRA is desirable. While this is in principle possible, the expected computational costs will be very high.

In the LCAO calculations, it is relatively simple to converge to a desired state or recognize that a state crossing has occurred at a particular field strength, due to the implementation of symmetry and the molecular overlap method (MOM) in CFOUR. The same is currently not yet true for the MRA calculations, making the comparison at larger field strengths more difficult, when the MRA and LCAO results differ significantly, as it is then not fully clear that both approaches have converged to the same state. The first next step will be the implementation of symmetry in the ZNEMO code of MADNESS for finer control over the target states and convergence behavior.

MRA provides the most general and easy access to highly accurate electronic structure calculations. Gaussian basis sets with isotropic exponents can have large errors, while GTOs with anisotropic exponents are rarely implemented or available. Finite-element methods for strong magnetic fields are only available for systems with cylindrical symmetry, while MRA allows computation of the full molecular PES in any orientation.

While an exhaustive investigation of a molecular system in a strong magnetic field using MRA only is currently not possible, it does provide an estimate of the basis set truncation error, which is one of the largest errors in a calculation. Also, MRA may serve as a reference for optimizing GTO basis sets for general molecules, for which it is the only available method.

SUPPLEMENTARY MATERIAL

Additional figures and tables as well as the CSV data files are provided as supplementary material.

ACKNOWLEDGMENTS

R.F. would like to thank the *Deutscher Akademischer Austauschdienst* (DAAD) for the financial support (Research Grants—Doctoral Programmes in Germany 2021/22; PID—57552340) and Mihkel Ugandi (HU Berlin) for useful discussions and for providing access to a nightly build of the HUMMR[74] code for the FCI calculations.

S.S. acknowledges support from the Deutsche Forschungsgemeinschaft (DFG) under Grant No. STO 1239/1-1.

AUTHOR DECLARATIONS

Conflict of Interest

The authors have no conflicts to disclose.

Author Contributions

Raunak Farhaz: Data curation (equal); Investigation (equal); Visualization (equal); Writing – original draft (equal); Writing – review & editing (equal). **Florian A. Bischoff**: Conceptualization (equal); Investigation (equal); Supervision (equal); Writing – original draft (equal); Writing – review & editing (equal). **Simon Blaschke**: Data curation (equal); Investigation (equal); Writing – original draft (equal); Writing – review & editing (equal). **Stella Stopkowicz**: Conceptualization (equal); Investigation (equal); Supervision (equal); Writing – original draft (equal); Writing – review & editing (equal).

DATA AVAILABILITY

The data that support the findings of this study are available within the supplementary material.

APPENDIX: TOTAL ENERGIES AND BASIS SET INCOMPLETENESS ERRORS

MRA total energies (E_{MRA}) and BSIE [$\Delta E = (E_{\mathrm{LCAO}} - E_{\mathrm{MRA}})$ in mE_{h}] of the **methylidyne radical (CH)** with respect to **unc-aug-cc-pV(D-5)Z** basis sets (*from left to right*) in parallel as well as perpendicular orientation, where the C_∞ axis is parallel and perpendicular, respectively, to the B-axis.

TABLE VI. MRA total energies (E_{MRA}) and BSIE [$\Delta E = (E_{\mathrm{LCAO}} - E_{\mathrm{MRA}})$ in mE_{h}] of **methylidyne radical (CH)** with respect to **unc-aug-cc-pV(D-5)Z** basis sets (*from left to right*) in parallel as well as perpendicular orientation, where the C_∞ axis is parallel and perpendicular, respectively, to the B-axis.

	MRA/E_{h}			ΔE (DZ)/mE_{h}			ΔE (TZ)/mE_{h}			ΔE (QZ)/mE_{h}			ΔE (5Z)/mE_{h}		
B/B_0	Doublet	Quartet	Sextet	Doublet	Quartet	Sextet	Doublet	Quartet	Sextet	Doublet	Quartet	Sextet	Doublet	Quartet	Sextet
Parallel orientation															
0.0	−38.284 588	−38.291 244	−37.847 622	8.0	8.6	7.9	2.0	2.0	2.5	0.4	0.4	0.8	0.0	0.0	0.5
0.1	−38.369 461	−38.427 760	−38.078 882	7.6	8.7	9.1	1.9	2.0	3.0	0.3	0.4	1.1	0.0	0.0	0.7
0.2	−38.429 548	−38.538 330	−38.281 543	8.6	9.2	10.6	2.0	2.1	3.2	0.4	0.4	1.1	0.0	0.0	0.7
0.5	−38.616 784	−38.783 303	−38.781 473	14.6	24.4	63.8	2.3	17.1	16.8	0.4	6.1	6.1	0.0	2.1	2.1
1.0	−38.618 818	−39.213 636	N.C.	30.3	113.1	⋯	3.0	11.9	⋯	0.7	5.4	⋯	0.0	2.5	⋯
2.0	−38.015 223	−39.733 233	N.C.	97.5	215.7	⋯	14.3	170.8	⋯	3.2	8.0	⋯	0.9	4.1	⋯
Perpendicular orientation															
0.0	−38.284 588	−38.291 244	−37.847 622	8.0	8.6	7.9	2.0	−2.0	2.5	0.4	0.4	0.8	0.0	0.0	0.5
0.1	−38.357 398	−38.427 992	−38.087 268	8.0	8.7	9.9	2.0	2.1	3.7	0.4	0.4	1.4	0.0	0.0	0.8
0.2	−38.434 840	−38.540 001	−38.319 491	8.4	9.1	10.3	2.0	2.1	3.4	0.4	0.4	1.3	0.0	0.0	0.7
0.5	−38.552 981	−38.844 130	−38.910 245	12.9	16.0	18.8	2.7	4.0	4.3	0.5	1.1	1.4	0.0	0.4	0.7
1.0	−38.480 883	−39.327 401	−39.846 342	41.5	51.2	155.6	4.4	5.4	32.1	1.7	2.0	13.3	0.7	0.9	6.4
2.0	−37.774 775	−39.763 742	−41.285 937	122.9	152.7	202.6	36.8	28.7	105.6	13.0	11.4	16.7	7.4	4.2	8.3

TABLE VII. MRA total energies (E_{MRA}) and BSIE [$\Delta E = (E_{LCAO} - E_{MRA})$ in mE_h] of **water (H_2O)** with respect to **unc-aug-cc-pV(D-5)Z** basis sets (*from left to right*) in parallel as well as perpendicular orientations, where the $\sigma_v(xy)$ is parallel and perpendicular, respectively, to the *B*-axis. For the triplet states at $B = 0.1$ and $B = 0.2$ of the water molecule in perpendicular orientation, see text.

	Parallel orientation														
	E_{MRA}/E_h			ΔE (DZ)/mE_h			ΔE (TZ)/mE_h			ΔE (QZ)/mE_h			ΔE (5Z)/mE_h		
B/B_0	Singlet	Triplet	Quintet	Singlet	Triplet	Quintet	Singlet	Triplet	Quintet	Singlet	Triplet	Quintet	Singlet	Triplet	Quintet
0.0	−76.068 177	−75.844 424	−75.390 317	24.3	24.2	24.7	5.8	5.8	6.0	1.3	1.5	2.3	0.1	0.4	1.2
0.1	−76.053 576	−75.929 453	−75.592 545	24.4	25.3	25.5	5.8	6.5	6.3	1.3	2.0	2.4	0.1	0.7	1.2
0.2	−76.010 498	−75.997 556	−75.783 635	24.7	29.6	27.2	5.8	8.2	6.9	1.3	2.7	2.7	0.1	1.1	1.5
0.5	−75.736 659	−76.185 644	−76.309 124	27.7	32.1	36.9	6.3	9.4	10.2	1.4	3.3	4.2	0.2	1.3	2.2
1.0	−75.188 475	−76.383 409	−76.898 383	72.1	62.6	80.6	13.5	11.0	14.1	5.2	3.8	4.9	3.1	2.1	2.7
2.0	−74.175 168	−76.226 869	−77.766 920	193.3	182.7	358.9	30.3	26.7	101.6	9.0	9.8	34.1	3.1	3.3	16.5
5.0	−67.298 188	−72.359 131	−77.365 484	1499.1	1279.5	1484.9	739.3	460.0	648.3	511.1	208.5	119.5	455.8	153.1	43.3
	Perpendicular orientation														
0.0	−76.068 177	−75.844 424	−75.390 318	24.3	24.2	24.8	5.8	5.8	6.0	1.3	1.5	2.3	0.1	0.4	1.2
0.1	−76.053 637	−75.847 849	−75.601 571	24.4	26.7	25.5	5.8	6.0	6.5	1.3	1.7	2.5	0.1	0.5	1.3
0.2	−76.011 154	−75.928 164	−75.809 918	24.6	33.1	26.4	5.9	8.6	6.9	1.3	2.9	2.8	0.1	1.1	1.5
0.5	−75.771 081	−76.153 866	−76.346 654	28.1	32.4	35.4	6.4	7.7	9.3	1.5	2.2	3.9	0.3	0.8	2.1
1.0	−75.470 536	−76.352 207	−76.949 846	51.7	68.7	73.3	8.5	11.3	11.3	2.9	3.4	4.0	1.2	2.6	2.0
2.0	−74.198 830	−76.187 634	−77.857 237	145.0	159.4	285.5	22.3	24.1	71.2	7.4	9.2	25.6	2.3	3.2	11.0
5.0	−67.052 379	−72.009 277	−77.124 019	1495.4	1028.2	1165.2	659.4	352.1	565.1	368.1	⋯	209.1	288.0	⋯	129.4

TABLE VIII. Energy difference (ΔE in mE_h) for the CH radical as well as H_2O with respect to change in normal coordinates at $B = 1.0B_0$ and having *sextet* and *quintet* spin multiplicities for CH and H_2O, respectively. The C_∞-axis and $\sigma_v(xy)$ plane for CH and H_2O, respectively, are **perpendicular** to the *B*-axis. The LCAO calculations were performed using the unc-aug-cc-pVTZ basis set (eq. = equilibrium of the field-free molecules).

	$\Delta E = (E_{LCAO} - E_{MRA})/mE_h$						
Normal modes	−0.6Q	−0.4Q	−0.2Q	Eq.	+0.2Q	+0.4Q	+0.6Q
	CH						
Symmetric stretching	37.4	35.5	33.8	32.1	30.1	28.3	27.0
	H_2O						
Symmetric bending	11.3	11.7	11.9	11.9	11.8	11.5	11.2
Symmetric stretching	25.6	19.7	15.1	11.9	9.9	8.8	8.2
Anti-symmetric stretching	14.7	13.2	12.2	11.9	12.2	13.2	14.7

MRA total energies (E_{MRA}) and BSIE [$\Delta E = (E_{LCAO} - E_{MRA})$ in mE_h] of **water (H_2O)** with respect to **unc-aug-cc-pV(D-5)Z** basis sets (*from left to right*) in parallel as well as perpendicular orientation, where the $\sigma_v(xy)$ is parallel and perpendicular, respectively, to the *B*-axis. For the triplet states at $B = 0.1$ and $B = 0.2$ of the water molecule in perpendicular orientation, see text.

Energy difference (ΔE in mE_h) for the CH radical as well as H_2O with respect to change in normal coordinates at $B = 1.0B_0$ for *sextet* and *quintet* spin multiplicities for CH and H_2O, respectively. The C_∞ axis and $\sigma_v(xy)$ plane for CH and H_2O, respectively, are **perpendicular** to the *B*-axis. The LCAO calculations were performed using the unc-aug-cc-pVTZ basis set (eq. = equilibrium of the field-free molecules).

Total energies (E_{MRA} and E_{LCAO}) for CH as well as H_2O with respect to change in normal coordinates at $B = 1.0B_0$ for *sextet* and *quintet* spin multiplicity for CH and H_2O, respectively. The C_∞ axis and $\sigma_v(xy)$ plane for CH and H_2O, respectively, are **perpendicular** to the *B*-axis. The LCAO calculations were performed using the unc-aug-cc-pVTZ basis set (eq. = equilibrium of the field-free molecules).

TABLE IX. Total energies (E_{MRA} and E_{LCAO}) for CH as well as H_2O with respect to change in normal coordinates at $B = 1.0B_0$ for *sextet* and *quintet* spin multiplicities for CH and H_2O, respectively. The C_∞-axis and $\sigma_v(xy)$ plane for CH and H_2O, respectively, are **perpendicular** to the *B*-axis. The LCAO calculations were performed using the unc-aug-cc-pVTZ basis set (eq. = equilibrium of the field-free molecules).

Method	Normal modes	−0.6Q	−0.4Q	−0.2Q	Eq.	+0.2Q	+0.4Q	+0.6Q
				CH				
E_{MRA}/E_h	Symmetric stretching	−39.491 014	−39.655 806	−39.768 031	−39.846 348	−39.900 945	−39.938 485	−39.963 406
E_{LCAO}/E_h	Symmetric stretching	−39.453 616	−39.620 317	−39.734 207	−39.814 226	−39.870 804	−39.910 147	−39.936 450
				H_2O				
E_{MRA}/E_h	Symmetric bending	−76.977 493	−76.962 747	−76.953 400	−76.950 424	−76.953 981	−76.963 218	−76.976 486
E_{LCAO}/E_h	Symmetric bending	−76.966 176	−76.951 051	−76.941 500	−76.938 510	−76.942 195	−76.951 682	−76.965 249
E_{MRA}/E_h	Symmetric stretching	−76.522 612	−76.723 527	−76.857 566	−76.950 424	−77.015 943	−77.062 076	−77.094 006
E_{LCAO}/E_h	Symmetric stretching	−76.496 974	−76.703 821	−76.842 475	−76.938 510	−77.006 029	−77.053 310	−77.085 842
E_{MRA}/E_h	Anti-symmetric stretching	−76.831 929	−76.904 389	−76.939 834	−76.950 424	−76.939 834	−76.904 390	−76.831 929
E_{LCAO}/E_h	Anti-symmetric stretching	−76.817 272	−76.891 186	−76.927 590	−76.938 510	−76.927 590	−76.891 186	−76.817 272

REFERENCES

[1] K. K. Lange, E. I. Tellgren, M. R. Hoffmann, and T. Helgaker, Science **337**, 327 (2012).
[2] P. Schmelcher, Science **337**, 302 (2012).
[3] D. Lai, Rev. Mod. Phys. **73**, 629 (2001).
[4] D. T. Wickramasinghe, G. Schmidt, L. Ferrario, and S. Vennes, Mon. Not. R. Astron. Soc. **332**, 29 (2002).
[5] M. A. Hollands *et al.*, Mon. Not. R. Astron. Soc. **520**, 3560 (2023).
[6] G. Wunner, H. Ruder, and H. Herold, Phys. Lett. A **85**, 430 (1981).
[7] H. Forster *et al.*, J. Phys. B: At., Mol. Phys. **17**, 1301–1319 (1984).
[8] W. Rosner, G. Wunner, H. Herold, and H. Ruder, J. Phys. B: At., Mol. Phys. **17**, 29 (1984).
[9] H. Friedrich and H. Wintgen, Phys. Rep. **183**, 37 (1989).
[10] U. Kappes and P. Schmelcher, J. Chem. Phys. **100**, 2878 (1994).
[11] H. Ruder, G. Wunner, H. Herold, and F. Geyer, *Atoms in Strong Magnetic Fields* (Springer Berlin Heidelberg, Berlin, Heidelberg, 1994).
[12] W. Becken, P. Schmelcher, and F. K. Diakonos, J. Phys. B: At., Mol. Opt. Phys. **32**, 1557 (1999).
[13] W. Becken and P. Schmelcher, J. Phys. B: At., Mol. Opt. Phys. **33**, 545 (2000).
[14] W. Becken and P. Schmelcher, Phys. Rev. A **63**, 053412 (2001).
[15] S. Lehtola, M. Dimitrova, and D. Sundholm, Mol. Phys. **118**, e1597989 (2020), arXiv:1812.06274 [physics].
[16] M. C. Miller and D. Neuhauser, Mon. Not. R. Astron. Soc. **253**, 107 (1991).
[17] A. Thirumalai and J. S. Heyl, Phys. Rev. A **89**, 052522 (2014).
[18] E. I. Tellgren, A. Soncini, and T. Helgaker, J. Chem. Phys. **129**, 154114 (2008).
[19] F. London, J. Phys. Radium **8**, 397 (1937).
[20] C. Aldrich and R. L. Greene, Phys. Status Solidi B **93**, 343 (1979).
[21] P. Schmelcher and L. S. Cederbaum, Phys. Rev. A **37**, 672 (1988).
[22] A. Kubo, J. Phys. Chem. A **111**, 5572 (2007).
[23] W. Zhu and S. B. Trickey, J. Chem. Phys. **147**, 244108 (2017).
[24] H. Åström and S. Lehtola, J. Phys. Chem. A **127**, 10872 (2023).
[25] S. Stopkowicz, J. Gauss, K. K. Lange, E. I. Tellgren, and T. Helgaker, J. Chem. Phys. **143**, 074110 (2015).
[26] R. J. Harrison *et al.*, SIAM J. Sci. Comput. **38**, S123 (2016).
[27] F. A. Bischoff, Phys. Rev. A **101**, 053413 (2020).
[28] S. F. Boys, Proc. R. Soc. London, Ser. A **200**, 542 (1950).
[29] T. Helgaker, "Molecular magnetic properties," in *European Summerschool of Quantum Chemistry—Book 2*, edited by S. Reine and T. Saue (Fotograph S.R.L., Stampatori Digitali, Palermo, 2017), Chap. 8, Vol. 12, p. 463.
[30] F. Hampe and S. Stopkowicz, J. Chem. Phys. **146**, 154105 (2017).
[31] F. Hampe and S. Stopkowicz, J. Chem. Theory Comput. **15**, 4036 (2019).
[32] F. Hampe, N. Gross, and S. Stopkowicz, Phys. Chem. Chem. Phys. **22**, 23522 (2020).
[33] S. Blaschke and S. Stopkowicz, J. Chem. Phys. **156**, 044115 (2022).
[34] M.-P. Kitsaras, L. Grazioli, and S. Stopkowicz, J. Chem. Phys. **160**, 094112 (2024).
[35] J. Austad, "Møller-Plesset theory to second order for the study of molecular systems in finite magnetic fields," Ph.D. thesis (University of Oslo, Oslo, Norway, 2013).
[36] E. I. Tellgren *et al.*, J. Chem. Phys. **140**, 034101 (2014).
[37] J. W. Furness *et al.*, J. Chem. Theory Comput. **11**, 4169 (2015).
[38] S. Reimann, A. Borgoo, E. I. Tellgren, A. M. Teale, and T. Helgaker, J. Chem. Theory Comput. **13**, 4089 (2017).
[39] C. Holzer *et al.*, J. Chem. Phys. **150**, 214112 (2019).
[40] C. Holzer, A. Pausch, and W. Klopper, Front. Chem. **9**, 746162 (2021).
[41] S. Sun and X. Li, J. Chem. Theory Comput. **16**, 4533 (2020).
[42] M. Wibowo, T. J. P. Irons, and A. M. Teale, J. Chem. Theory Comput. **17**, 2137 (2021).
[43] T. Culpitt, L. D. M. Peters, E. I. Tellgren, and T. Helgaker, J. Chem. Phys. **155**, 024104 (2021).
[44] L. D. M. Peters, T. Culpitt, L. Monzel, E. I. Tellgren, and T. Helgaker, J. Chem. Phys. **155**, 024105 (2021).
[45] B. S. Ofstad *et al.*, J. Chem. Phys. **159**, 204109 (2023).
[46] R. J. Harrison, G. I. Fann, T. Yanai, Z. Gan, and G. Beylkin, J. Chem. Phys. **121**, 11587 (2004).
[47] B. Alpert, G. Beylkin, D. Gines, and L. Vozovoi, J. Comput. Phys. **182**, 149 (2002).
[48] F. A. Bischoff, "Computing accurate molecular properties in real space using multiresolution analysis," in *Advances in Quantum Chemistry* (Elsevier, 2019).
[49] G. Beylkin and M. J. Mohlenkamp, SIAM J. Sci. Comput. **26**, 2133 (2005).
[50] T. Yanai, G. I. Fann, Z. Gan, R. J. Harrison, and G. Beylkin, J. Chem. Phys. **121**, 6680 (2004).
[51] T. Yanai, G. I. Fann, Z. Gan, R. J. Harrison, and G. Beylkin, J. Chem. Phys. **121**, 2866 (2004).
[52] F. A. Bischoff, J. Chem. Phys. **146**, 124126 (2017).
[53] T. Yanai, R. J. Harrison, and N. C. Handy, Mol. Phys. **103**, 413 (2005).
[54] J. S. Kottmann, S. Höfener, and F. A. Bischoff, Phys. Chem. Chem. Phys. **17**, 31453 (2015).
[55] F. A. Bischoff and E. F. Valeev, J. Chem. Phys. **139**, 114106 (2013).
[56] J. S. Kottmann and F. A. Bischoff, J. Chem. Theory Comput. **13**, 5945 (2017).
[57] J. S. Kottmann and F. A. Bischoff, J. Chem. Theory Comput. **13**, 5956 (2017).
[58] J. B. Stückrath and F. A. Bischoff, J. Chem. Theory Comput. **17**, 1408 (2021).

[59]J. Anderson, B. Sundahl, R. Harrison, and G. Beylkin, J. Chem. Phys. **151**, 234112 (2019).
[60]L. Fabian, K. Stefan, and S. K. Jakob, "The advent of fully variational quantum eigensolvers using a hybrid multiresolution approach," arXiv:2410.19116 (2024).
[61]LONDON, a quantum-chemistry program for plane-wave/GTO hybrid basis sets and finite magnetic field calculations by E. I. Tellgren (primary author), T. Helgaker, A. Soncini, K. K. Lange, A. M. Teale, U. Ekström, S. Stopkowicz, J. H. Austad, and S. Sen, see londonprogram.org for more information.
[62]CFOUR, Coupled-Cluster techniques for Computational Chemistry, a quantum-chemical program package, With contributions from J. F. Stanton, A. Asthana, A. A. Auer, R. J. Bartlett, U. Benedikt, C. Berger, D. E. Bernholdt, S. Blaschke, Y. J. Bomble, S. Burger, O. Christiansen, D. Datta, F. Engel, R. Faber, J. Greiner, M. Heckert, O. Heun, M. Hilgenberg, C. Huber, T.-C. Jagau, D. Jonsson, J. Jusélius, T. Kirsch, M.-P. Kitsaras, K. Klein, G. M. Kopper, W. J. Lauderdale, F. Lipparini, J. Liu, T. Metzroth, L. A. Mück, D. P. O'Neill, T. Nottoli, J. Oswald, D. R. Price, E. Prochnow, C. Puzzarini, K. Ruud, F. Schiffmann, W. Schwalbach, C. Simmons, S. Stopkowicz, A. Tajti, T. Uhlířová, J. Vázquez, F. Wang, J. D. Watts, P. Yergün, C. Zhang, X. Zheng, the integral packages MOLECULE, J. Almlöf, P. R. Taylor, PROPS, P. R. Taylor, ABACUS, T. Helgaker, H. J. Aa. Jensen, P. Jørgensen, J. Olsen, ECP routines, A. V. Mitin, C. van Wüllen *et al.*, For the current version, see http://www.cfour.de.
[63]D. A. Matthews *et al.*, J. Chem. Phys. **152**, 214108 (2020).
[64]T. H. Dunning, Jr., J. Chem. Phys. **90**, 1007 (1989).
[65]R. A. Kendall, T. H. Dunning, Jr., and R. J. Harrison, J. Chem. Phys. **96**, 6796 (1992).
[66]D. E. Woon and T. H. Dunning, Jr., J. Chem. Phys. **100**, 2975 (1994).
[67]MADNESS, Multiresolution adaptive numerical environment for scientific simulation; https://github.com/m-a-d-n-e-s-s/madness.
[68]F. A. Bischoff, J. Chem. Phys. **141**, 184105 (2014).
[69]J. Austad, A. Borgoo, E. I. Tellgren, and T. Helgaker, Phys. Chem. Chem. Phys. **22**, 23502 (2020).
[70]S. Thomas, F. Hampe, S. Stopkowicz, and J. Gauss, Mol. Phys. **119**, e1968056 (2021).
[71]A. T. B. Gilbert, N. A. Besley, and P. M. W. Gill, J. Phys. Chem. A **112**, 13164 (2008).
[72]G. David, T. J. P. Irons, A. E. A. Fouda, J. W. Furness, and A. M. Teale, J. Chem. Theory Comput. **17**, 5492 (2021).
[73]M.-P. Kitsaras, "Finite magnetic-field coupled-cluster methods: Efficiency and utilities," Ph.D. thesis (Johannes Gutenberg-Universität Mainz, Mainz, Germany, 2023).
[74]M. Ugandi and M. Roemelt, J. Comput. Chem. **44**, 2374 (2023).
[75]A. Thirumalai, "Hydrogen and helium atoms in intense magnetic fields coupled with high pressure in neutron star atmospheres," J. Phys. Chem. A **129**(9), 2161–2172 (2025).